Frequency-domain method for measuring spectral properties in multiple-scattering media: methemoglobin absorption spectrum in a tissuelike phantom

Joshua B. Fishkin, Peter T. C. So, Albert E. Cerussi, Sergio Fantini, Maria Angela Franceschini, and Enrico Gratton

We have measured the optical absorption and scattering coefficient spectra of a multiple-scattering medium (i.e., a biological tissue-simulating phantom comprising a lipid colloid) containing methemoglobin by using frequency-domain techniques. The methemoglobin absorption spectrum determined in the multiple-scattering medium is in excellent agreement with a corrected methemoglobin absorption spectrum obtained from a steady-state spectrophotometer measurement of the optical density of a minimally scattering medium. The determination of the corrected methemoglobin absorption spectrum takes into account the scattering from impurities in the methemoglobin solution containing no lipid colloid. Frequency-domain techniques allow for the separation of the absorbing from the scattering properties of multiple-scattering media, and these techniques thus provide an absolute measurement of the optical absorption spectra of the methemoglobin/lipid colloid suspension. One accurately determines the absolute methemoglobin absorption spectrum in the frequency domain by extracting the scattering and absorption coefficients from the phase shift Φ and average light intensity DC (or Φ and the amplitude of the light-intensity oscillations AC) data with relationships provided by diffusion theory, but one determines it less accurately by using the Φ and modulation M ($M \equiv AC/DC$) data and the diffusion theory relationships. In addition to the greater uncertainty in the absorption and scattering coefficients extracted from the Φ and M data, the optical parameters extracted from the Φ and M data exhibit systematically inaccurate behavior that cannot be explained by random noise in the system. Possible reasons for the systematically lower accuracy of the methemoglobin absorption spectrum obtained from Φ and M data are discussed.

1. Introduction

The determination of the optical properties of turbid biological media is a challenging problem in several areas of medicine and biotechnology.[1–8] The intent of this study is to determine the conditions in which the accurate and efficient determination of these optical properties is possible by frequency-domain techniques. Frequency-domain techniques consist of sinusoidally modulating the intensity of a light source (Fig. 1) and employing a phase-sensitive detection system to measure the amplitude of the light-intensity oscillations AC, average light intensity DC, and phase shift Φ of the detected light-intensity signal relative to the source. We must remember that in the frequency-domain method, only the front of the light-intensity wave is considered, not the optical light front, which is multiply scattered in a turbid medium and typically has a frequency that is of the order of 10^6 times greater than the light-source intensity-modulation frequency. Gratton *et al.*[9] proposed using a frequency-domain diffusion model to describe light emitted into a turbid medium from a sinusoidally modulated point source. Fishkin *et al.*[10] demonstrated that when intensity-modulated light is emitted from a point source into a quasi-infinite turbid medium, a spherically symmetric photon-density wave is launched. Since then, phase shift and/or demodulation data [demodulation ≡

The authors are with the Laboratory for Fluorescence Dynamics, Department of Physics, University of Illinois at Urbana-Champaign, 1110 West Green Street, Urbana, Illinois 61801. S. Fantini and M. A. Franceschini are on leave from the Istituto di Elettronica Quantistica, Consiglio Nazionale delle Ricerche, Via Panciatichi, 56/30, 50127 Florence, Italy.

Received 2 May 1994; revised manuscript received 28 July 1994.
0003-6935/95/071143-13$06.00/0.

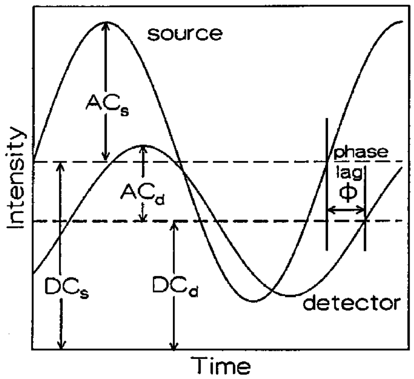

Fig. 1. Time evolution of the intensity from a sinusoidally intensity-modulated source. The detected photon-density wave retains the same modulation frequency as the source photon-density wave but is delayed because of the phase velocity of the wave in the medium. The reduced amplitude of the detected wave arises from attenuation related to scattering and absorption processes. The demodulation is the ratio AC/DC at the detector normalized to the modulation of the source.

$[(AC/DC)_{\text{detector}}/(AC/DC)_{\text{source}}]$ have been used typically in the frequency domain to determine the absorption and scattering coefficients of turbid media.[11–16] Patterson *et al.*[17] suggested using the phase-shift and DC data as an alternative to the phase-shift and demodulation data for determining these parameters when the demodulation of the detected light-intensity signal is close to one: They show that in these circumstances, typical uncertainties in the demodulation data and phase-shift data yield greater uncertainties in the calculated absorption and scattering coefficients than those yielded by typical uncertainties in the DC data and phase-shift data.

Our endeavor in this study is threefold: (1) Our primary goal is to separate completely the light-absorbing from the light-scattering properties of a tissuelike phantom containing a small concentration of methemoglobin. We cover a broad spectral range in this study, from the green to the red portion of the visible spectrum. (2) We wish to determine which combination of phase shift, AC, DC, and demodulation data yields the most accurate and precise calculation of the absorption and scattering coefficient spectra of this medium. (3) We wish to know the smallest data set that typically allows for accurate determination of these spectra, that is, at what minimum number of light-source/light-detector separations and light-source intensity-modulation frequencies can AC, DC, and phase-shift data be acquired to yield accurate absorption and scattering coefficients. The smaller the data set, the more efficient (i.e., rapid) the determination of the absorption and scattering coefficient spectra for a turbid medium. Fantini *et al.*[18] used frequency-domain techniques in conjunction with a diffusion model for light propagation to obtain reasonably accurate absorption spectra for different concentrations of the absorbing dye methylene blue in a multiple-scattering medium. However, they were constrained by the low power and limited response time of their light-emitting diode source to a limited range of source/detector separations and modulation frequencies. We wish to know if the quality of the spectra may be improved through calculations from a data set at least 10 times larger than that obtained by Fantini *et al.* Our data were obtained at multiple modulation frequencies ranging across more than a decade of values and at multiple source/detector separations.

The data analysis we use to determine the absorption and scattering spectra of a turbid medium is based on a diffusion approximation to the Boltzmann transport equation. We then determine the absorption and scattering coefficient spectra of our macroscopically uniform turbid medium containing a known concentration of methemoglobin (i.e., ferric hemoglobin) by fitting different combinations of phase-shift, AC, and DC data obtained at different light wavelengths to a frequency-domain diffusion model derived by Fishkin and Gratton.[19] At a given light wavelength, these frequency-domain data were acquired at multiple source/detector separations, with multiple light-source intensity-modulation frequencies at each source/detector separation. The light wavelengths used covered the green to red region of the visible spectrum, and the source intensity was modulated at radio frequency in the 19.05–304.80-MHz region. We obtained the contribution of the methemoglobin to the absorption spectrum of this turbid medium by comparing the absorption spectrum of the turbid medium to the absorption spectrum of a medium of the same turbidity containing no methemoglobin (i.e., a blank or control turbid medium). The absorption and scattering coefficient spectra of the control turbid medium were obtained through the same experimental protocol as the turbid medium containing the methemoglobin.

The accuracy in determining the concentration contribution of methemoglobin to the absorption spectrum of the uniform turbid medium was then evaluated: The apparent absorption spectrum $[\mu_a]_{\text{app}}$ of an equal concentration of methemoglobin in an aqueous solution of minimal turbidity was compared with the methemoglobin absorption spectrum obtained from the turbid medium. We determined this apparent absorption coefficient by a steady-state measurement of the medium optical density, using a transmission geometry and the Beer–Lambert relationship:

$$[\mu_a]_{\text{app}} \equiv \mu_a + \mu_s \cong \frac{1}{L} \log_e \frac{I_0}{I} \equiv \epsilon[C], \tag{1}$$

where μ_a is the inverse of the mean distance a photon travels before it is absorbed by the chromophore (the chromophore being methemoglobin in this case), μ_s is the inverse of the mean free path for elastic scattering of a photon by the chromophore, L is the distance the photons traveled through the transporting medium before reaching the detector, I_0 is the incident light intensity, I is the detected light intensity, ϵ is the extinction coefficient of the chromophore at light wavelength λ (in units of $\text{cm}^{-1}\ \mu\text{M}^{-1}$), and $[C]$ is the concentration of the chromophore. Equation (1) is valid if the following assumption holds: $1/\mu_s \gg L$ so that the probability of multiple scattering of photons in the transporting medium is negligible; all photons reaching the detector thereby travel the same distance L through the medium. The steady-state expression in Eq. (1) may be derived from the Boltzmann transport equation[20,21] if it is assumed that μ_s is sufficiently small that the integral term in the Boltzmann transport equation can be neglected. Equation (1) becomes an exact relationship when $\mu_s = 0$. Equation (1) is not applicable to the case of diffusive light transport through a turbid medium of width L. In these circumstances, $\mu_a \ll \mu_s$, and $1/\mu_s \ll L$ so that the probability of multiple scattering of photons in the medium is high. Hence we cannot assume that all the photons traversing the medium travel the same distance L from the source to the detector.

2. Theory

For an infinite, macroscopically uniform medium, Fishkin and Gratton[19] solved the diffusion equation with a sinusoidally intensity-modulated point source for the photon density $U(r, t)$ at a location r relative to the source at time t to yield (in photons per unit volume)

$$U(r,t) = \frac{S}{4\pi v D r}\exp\left[-r\left(\frac{\mu_a}{D}\right)^{1/2}\right] + \frac{SA}{4\pi v D r} \times \exp\left\{-r\left(\frac{v^2{\mu_a}^2 + \omega^2}{v^2 D^2}\right)^{1/4}\cos\left[\frac{1}{2}\tan^{-1}\left(\frac{\omega}{v\mu_a}\right)\right]\right\} \times \exp\left\{ir\left(\frac{v^2{\mu_a}^2 + \omega^2}{v^2 D^2}\right)^{1/4} \times \sin\left[\frac{1}{2}\tan^{-1}\left(\frac{\omega}{v\mu_a}\right)\right] - i(\omega t + \epsilon)\right\}. \quad (2)$$

The speed of each photon in the medium surrounding the scattering particles is given by $v = (3.00 \times 10^{10}$ cm/s)/n, n being the index of refraction of the transporting medium.

$$D \equiv \frac{1}{3(\mu_a + \mu_s')} \quad (3)$$

is the diffusion coefficient in units of distance, μ_a is the absorption coefficient [defined in Eq. (1)],

$$\mu_s' \equiv (1 - g)\mu_s \quad (4)$$

is the reduced scattering coefficient, where g is the average of the cosine of the scattering angle, and μ_s is the scattering coefficient [defined in Eq. (1)]. S is the source strength (in photons per second), A is the modulation of the source, $i \equiv (-1)^{1/2}$, ω is the angular modulation frequency of the source, and ϵ is the phase of the source. From Eq. (2) we predict that the photon density $U(r, t)$ generated by an isotropically emitting, sinusoidally intensity-modulated point source immersed in an infinite medium constitutes a scalar field that propagates at a constant speed in a spherical wave and attenuates as a decaying exponential in r, divided by r, as it propagates.

Figure 2 shows a typical geometry used to generate and detect the diffusive wave predicted by Eq. (2). Although the photons represented in Fig. 2 are injected into the multiply scattering medium in the direction $-\hat{\Omega}_d$, we assume in the manner of Patterson *et al.*[22] that photons injected into the medium are initially scattered at a distance of $1/(\mu_a + \mu_s')$ (i.e., one mean free path) from the end of the source optical fiber. The assumption is that these first interactions are sufficiently localized that a simple Dirac-delta function accurately describes the light propagation when $r \gg 1/\mu_s'$. Fishkin and Gratton[19] confirmed the r dependence of Eq. (2) for a quasi-infinite skim-milk medium containing an 810-nm light source modulated at 120 MHz, using the source/detector geometry shown in Fig. 2, with data acquired at r values varying from 2.5 to 9.6 cm in 0.115-cm increments.

The source terms S, A, and ϵ are obviously independent of the quantities of interest, namely, the absorption and scattering coefficients $[\mu_a(\lambda), \mu_s'(\lambda)]$ of the medium at some light wavelength λ. Ideally the source terms are also independent of ω, but in practice they are not. One possibility that eliminates these source terms from a measurement at a given ω is to measure the properties of the photon density at two different source/detector separations, namely, r and r_0, and compare the quantities obtained at these two distances. Equation (2) yields expressions for quantities obtained at r relative to the corresponding quantities obtained at r_0, namely, the steady-state photon density DC, the amplitude of the

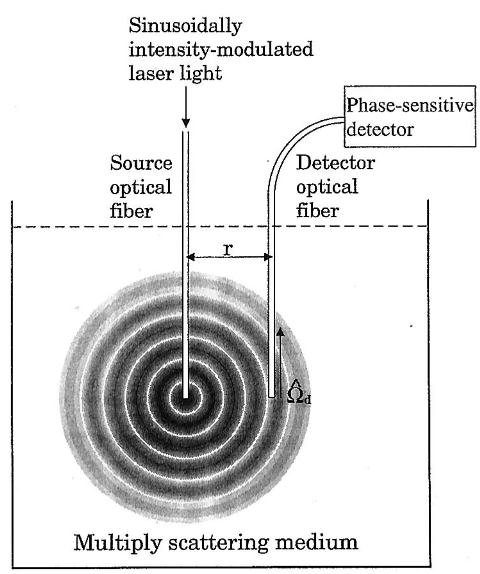

Fig. 2. Typical geometry used to generate and detect a diffusive photon-density wave. $\hat{\Omega}_d$ is the principal direction in which photons can enter the detector optical fiber. We assume that a Dirac-delta function $\delta(r)$ accurately describes the light source when $r \gg 1/\mu_s'$.

photon-density oscillations AC, and the phase shift of the photon-density wave Φ. The relative quantities are given by

$$DC_{\rm rel} \equiv \frac{DC(r)}{DC(r_0)} = \frac{r_0}{r} \exp\left[-(r - r_0)\left(\frac{\mu_a}{D}\right)^{1/2}\right], \tag{5}$$

$$AC_{\rm rel} \equiv \frac{AC(r)}{AC(r_0)} = \frac{r_0}{r} \exp\left\{-(r - r_0)\left(\frac{v^2\mu_a{}^2 + \omega^2}{v^2D^2}\right)^{1/4} \times \cos\left[\frac{1}{2}\tan^{-1}\left(\frac{\omega}{v\mu_a}\right)\right]\right\}, \tag{6}$$

$$\Phi_{\rm rel} \equiv \Phi(r) - \Phi(r_0) = (r - r_0)\left(\frac{v^2\mu_a{}^2 + \omega^2}{v^2D^2}\right)^{1/4} \times \sin\left[\frac{1}{2}\tan^{-1}\left(\frac{\omega}{v\mu_a}\right)\right]. \tag{7}$$

The relative demodulation of the photon-density wave is given by

$$M_{\rm rel} \equiv AC_{\rm rel}/DC_{\rm rel}. \tag{8}$$

Our frequency-domain data are obtained in a manner that allows for fitting these data (i.e., $DC_{\rm rel}$, $AC_{\rm rel}$, $\Phi_{\rm rel}$, and $M_{\rm rel}$) directly to Eqs. (5)–(8) to obtain the absorption and reduced scattering coefficients $[\mu_a(\lambda)$, $\mu_s'(\lambda)]$ of the multiple-scattering medium at some light wavelength λ. Note that in the three equations [Eqs. (5)–(7)], there are only two unknowns, namely, $v\mu_a$ and vD, where D is given by Eq. (3). (We assume that the index of refraction of the transporting medium is known, so that explicit values for μ_a and μ_s' can be recovered from the quantities $v\mu_a$ and vD.) This means that in principle only two out of the three expressions in Eqs. (5)–(7) are needed to determine $\mu_a(\lambda)$ and $\mu_s'(\lambda)$ at a single modulation frequency $\omega/2\pi$. Fantini *et al.*[18] have calculated explicit expressions for μ_a, μ_s' and their relative uncertainties by using different combinations of Eqs. (5)–(7).

We may obtain explicit analytical expressions for μ_s' in terms of μ_a from Eqs. (5)–(7) by employing the trigonometric identities

$$\sin\frac{\beta}{2} = \left(\frac{1 - \cos\beta}{2}\right)^{1/2}, \quad \cos\frac{\beta}{2} = \left(\frac{1 + \cos\beta}{2}\right)^{1/2}, \tag{9}$$

where

$$\beta \equiv \tan^{-1}\left(\frac{\omega}{v\mu_a}\right). \tag{10}$$

Equation (3) with Eqs. (5)–(10) yields the following:

$DC_{\rm rel}$ equation,

$$\mu_s' = \frac{1}{3\mu_a}\left[\frac{\ln(r/r_0\, DC_{\rm rel})}{r - r_0}\right]^2 - \mu_a; \tag{11}$$

$AC_{\rm rel}$ equation,

$$\mu_s' = \frac{2}{3\mu_a}\left[\frac{\ln(r/r_0\, AC_{\rm rel})}{r - r_0}\right]^2\left\{\left[1 + \left(\frac{\omega}{v\mu_a}\right)^2\right]^{1/2} + 1\right\}^{-1} - \mu_a; \tag{12}$$

$\Phi_{\rm rel}$ equation,

$$\mu_s' = \frac{2}{3\mu_a}\left[\frac{\Phi_{\rm rel}}{r - r_0}\right]^2\left\{\left[1 + \left(\frac{\omega}{v\mu_a}\right)^2\right]^{1/2} - 1\right\}^{-1} - \mu_a; \tag{13}$$

$M_{\rm rel}$ equation,

$$\mu_s' = \frac{1}{3\mu_a}\left[\frac{\ln(M_{\rm rel})}{r - r_0}\right]^2 \times \left(1 - \frac{1}{\sqrt{2}}\left\{\left[1 + \left(\frac{\omega}{v\mu_a}\right)^2\right]^{1/2} + 1\right\}^{1/2}\right)^{-2} - \mu_a; \tag{14}$$

For an ideal system represented by Eqs. (11)–(14), a measurement of $DC_{\rm rel}$, $AC_{\rm rel}$, $\Phi_{\rm rel}$, and $M_{\rm rel}$ in a multiply scattering medium at a single modulation frequency $\omega/2\pi$ should be such that Eqs. (11)–(14), in the employment of these measured quantities, yield plots of μ_s' versus μ_a that intersect at the same point.

3. Experimental Apparatus and Method

3.A. Light Source, Fiber Optics, and Detectors for a Frequency-Domain Measurement

Two light sources, shown in Fig. 3, were used in the frequency-domain experiments. One of the light sources is a mode-locked Nd:YAG laser (Coherent Antares 76-S) that produces a train of equally spaced

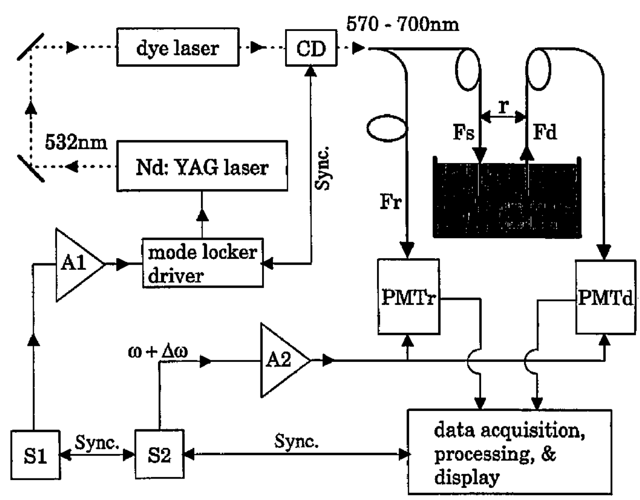

Fig. 3. Schematic of the frequency-domain spectrophotometer used for measurements of the optical properties of turbid media. S1, S2, frequency synthesizers (PTS 500, Programmed Test Sources, Inc., and Marconi Instruments Signal Generator 2022A, respectively); A1, Hewlett-Packard 8447E amplifier; A2, Electronic Navigation Industry 603L rf amplifier. The mode-locker driver is from Coherent Model 7600. CD, cavity dumper (Coherent 7200). Synthesizers S1 and S2 are phase locked to the data acquisition, processing, and display portion of the instrument. Modulation frequencies range from 19.05 to 304.8 MHz. The cross-correlation frequency is 40 Hz.

light pulses with a repetition rate of 76.20 MHz and with its output frequency doubled to a wavelength of 532 nm. The other light source is a dye laser (Coherent 700 dye laser, Palo Alto, Calif.) that is synchronously pumped by the 532-nm, 76.20-MHz output of the above-mentioned Nd:YAG system. The dye laser output is cavity dumped (by a Coherent 7200 cavity dumper) to yield a train of equally spaced light pulses with a repetition rate of 19.05 MHz, with the train of pulses from the dye laser supplying an average power of ~50 mW. Each pulse is ~5 ps full width at half-maximum. With the particular laser dyes utilized in the dye laser, namely, a Rhodamine 6G dye and a DCM dye (Exciton, Inc., Dayton, Ohio), the visible light obtained from the dye laser was continuously tunable over the wavelength range of 570–700 nm. Fourier analysis of the 19.05-MHz (76.20-MHz) light-pulse train yields a series of harmonic intensity-modulation frequencies with a spacing of 19.05 MHz (76.20 MHz) between each frequency.[23] Cross-correlation techniques permit precise isolation of individual intensity-modulation frequencies.[23,24] When measurements were performed with the 532-nm light, the average power of the 76.20-MHz pulse train was attenuated to 100 mW by transmission through a polarizer.

The 19.05-MHz (76.20-MHz) light-pulse train is coupled to a plastic bifurcated optical fiber, as shown in Fig. 3. One of the ends of this fiber conveys the laser light to the sample being studied (i.e., fiber Fs, the source, or sample optical fiber), and the other fiber end (i.e., fiber Fr, the reference optical fiber) conveys the light to a reference Hamamatsu R928 photomultiplier tube (PMTr). The bifurcation of the optical fibers is such that most of the laser light injected into the common end of the bifurcated optical fibers is transmitted to the scattering medium through fiber Fs with only a small fraction of the light going to PMTr through fiber Fr. The aperture diameter of optical fiber Fs is 0.15 cm, and the aperture diameter of optical fiber Fr is 0.1 cm. The detector optical fiber (i.e., fiber Fd) consists of a bundle of glass optical fibers with an overall aperture diameter of 0.3 cm whose output is detected by another Hamamatsu R928 photomultiplier tube (PMTd). PMTr is used as a reference for phase-shift measurements. A digital acquisition method processed the cross-correlated signal from the photomultiplier detector electronics.[24] In our measurements the cross-correlation frequency was $\Delta\omega/2\pi = 40$ Hz. The geometrical configuration of the detector optical fiber with respect to the source optical fiber (Figs. 2 and 3) was such that most of the detected photons were scattered at right angles relative to the source/detector separation r. The multiply scattering media being studied were held in a glass container measuring 19 cm in diameter by 10 cm in height. The ends of optical fibers Fs and Fd (with a maximum separation distance of 3.0 cm) were immersed in the multiple-scattering medium as far as possible from the medium boundaries in order to best approximate the infinite medium boundary condition.

3.B. Measurement Technique in Multiple-Scattering Media

Frequency-domain measurements on the scattering media were made at 28 different light-source wavelengths λ, namely, at 532 nm and at wavelengths that range from 570 to 700 nm in 5-nm increments. At each light-source wavelength between 570 and 700 nm, measurements of phase shift Φ, AC, and DC were made at five different intensity-modulation frequencies at source/detector separations of 2.0, 2.5, and 3.0 cm with the intensity-modulation frequencies ranging from 19.05 to 247.65 MHz. The source/detector separation r was controlled by a raster scanning device (Techno XYZ positioning table, New Hyde Park, N.Y.) with the uncertainty of a change in r equal to 10 μm. At the 532-nm wavelength the source/detector distances were the same but measurements were made at four different intensity-modulation frequencies ranging from 76.20 to 304.80 MHz. The DC, AC, and phase-shift Φ quantities measured at the $r = 2.5$-cm and $r = 3.0$-cm source/detector distances at a given intensity-modulation frequency $\omega/2\pi$ were made relative to the corresponding quantities measured at the $r_0 = 2.0$-cm source/detector separation (at the same modulation frequency). As mentioned above, the measurement of the relative DC, AC, and phase-shift quantities (i.e., DC_{rel}, AC_{rel}, and Φ_{rel}) at a given value of $\omega/2\pi$ has the following advantage: Terms that are dependent on the source but independent of the parameters of the medium in which we are interested are eliminated, as are the spectral response factors of the phase-sensitive detection system. When fitting our frequency-domain data (DC_{rel}, AC_{rel}, and Φ_{rel}) to Eqs. (5)–(8) to obtain the medium absorption and scattering coefficients $[\mu_a(\lambda), \mu_s'(\lambda)]$ at some light wavelength λ, we assume that $n = 1.33$ for the multiple-scattering media being investigated (which is the index of refraction of water in the spectral region considered). Typical instrumental uncertainties in a frequency-domain measurement are $\pm 0.3\%$ for both DC_{rel} and AC_{rel}, $\pm 0.4\%$ for M_{rel}, and $\pm 0.2°$ for Φ_{rel}.[25]

3.C. Absorbing Material and Scattering Medium

Methemoglobin (i.e., ferric hemoglobin) was selected as a test of a biologically important absorbing material. The advantage of using methemoglobin for these experiments is that it does not change into another form of hemoglobin while exposed to air at room temperature during a measurement. The methemoglobin solutions are brown, and the compound has a four-banded absorption spectrum with a band in the orange-red at 630 nm.[26] We prepared a stock solution containing a 100-μM concentration of methemoglobin by dissolving equal concentrations of horse hemoglobin (Sigma Chemical Company, St. Louis, Mo.) and potassium ferricyanide into an aqueous solution buffered at a pH of 7.23. (We prepared the buffered aqueous solution by dissolving a 50-mM concentration of sodium phosphate dibasic in water and then adding a sufficient amount of hydrochloric acid so that the scattering medium was buffered at a pH of 7.23.) The potassium ferricyanide converted the balance of the hemoglobin that was not already in the methemoglobin form into methemoglobin. The resultant methemoglobin form was stable during all the experiments. A quantity of 0.075 mL of the 100-μM stock methemoglobin solution was then combined with 2.925 mL of the 7.23 pH buffer to give a 2.5-μM concentration of methemoglobin. We then measured the apparent absorption spectrum of this sample at room temperature between wavelengths of 532 and 700 nm by employing a transmission geometry, where the width of the sample-holding cuvette was 1 cm. The $[\mu_a]_{app}$ spectrum shown in Fig. 4 is obtained by inserting the measured optical density and the width of the sample-holding cuvette into Eq. (1). [Optical density, which is defined as $\log_{10}(I_0/I)$, must be converted to $\log_e(I_0/I)$ to employ Eq. (1).] A standard steady-state spectrophotometer (Perkin-Elmer Lambda 5, The Perkin-Elmer Corporation, St. Louis, Mo.) was used to obtain this spectrum, which is used for quantitative comparison with the methemoglobin absorption spectrum measured in a multiple-scattering medium.

We prepared 2300 mL of the scattering medium containing no methemoglobin (a blank scattering medium) by combining 177 mL of Liposyn III 20% with 2123 mL of the above-mentioned 7.23 pH buffer. This mixture of Liposyn and buffer yields a medium scattering coefficient of $\sim$20 cm^{-1}, which is typical for soft tissues.[27] The solids content of this medium was 1.54% Liposyn. The absolute absorption and scattering coefficient spectra of this medium were determined through the frequency-domain measurement technique described in Subsection 3.B and Section 4, and these spectra are presented in Fig. 5. We then uniformly mixed 59 mL of the above-mentioned 100-μM stock solution of methemoglobin with 2300 mL of the scattering medium to give a 2359-mL solution containing a 2.5-μM concentration of methemoglobin with a solids content of 1.50% Liposyn. The absolute absorption and scattering coefficient spectra of this medium were then deter

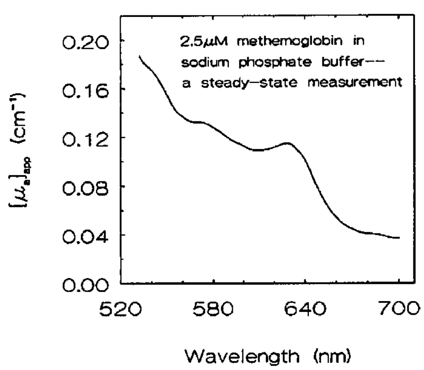

Fig. 4. Apparent absorption spectrum of a 2.5-μM solution of methemoglobin in a 50-mM sodium phosphate buffer of 7.23 pH. A transmission geometry in a sample-holding cuvette of 1-cm width and Eq. (1) allowed for the determination of this spectrum through measurement of the optical density of the medium.

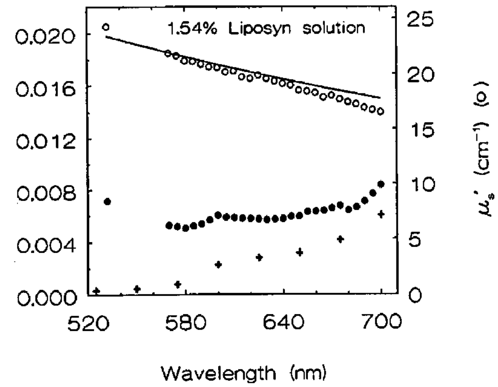

Fig. 5. Frequency-domain-determined scattering and absorption of a Liposyn III blank or reference medium. The solids content of this medium is 1.54% Liposyn. We determined the absolute absorption coefficients μ_a (●) and absolute reduced scattering coefficients μ_s' (○) by simultaneously fitting DC_{rel} and Φ_{rel} data, obtained at two relative distances (i.e., $r = 2.5$ and 3.0 cm relative to $r_0 = 2.0$ cm) at multiple modulation frequencies ranging from 19.05 to 304.80 MHz, to Eqs. (5) and (7), respectively. The uncertainties in the μ_a and μ_s' values recovered from the data analysis are of the order of 2×10^{-5} and 0.1 cm^{-1}, respectively. Absorption of water (+) is as given by Hale and Querry.[29] The Mie theory calculations of van Staveren *et al.*[30] (solid curve) are for a medium consisting of a solids content of 1.54% Intralipid.

mined through our frequency-domain methodology, and the absorption spectrum obtained from the above-mentioned blank scattering medium was then subtracted from the absorption spectrum of this 2.5-μM methemoglobin/1.50% Liposyn/7.23 pH aqueous buffer medium. Thus the absolute absorption spectrum of 2.5 μM of methemoglobin was recovered from the multiply scattering medium. This absorption spectrum along with the measured reduced scattering coefficient spectrum of the medium is shown in Figs. 6 and 7.

4. Results

The absolute absorption coefficients $\mu_a(\lambda)$ and absolute reduced scattering coefficients $\mu_s'(\lambda)$ represented, respectively, by the solid and open circles in Figs. 5–7 are extracted from the frequency-domain data obtained at each light-source wavelength λ through a nonlinear least-squares fitting routine designed to fit multiple sets of data simultaneously.[28] This fitting routine, originally designed to fit frequency-domain fluorescence decay data, has been specifically modified to fit the data obtained at a given λ at multiple modulation frequencies $\omega/2\pi$ and multiple relative source/detector separations $(r - r_0)$ to different pairings of Eqs. (5)–(8). The $\mu_a(\lambda)$ and $\mu_s'(\lambda)$ parameters were extracted from frequency-domain data sets obtained at given λ values in three different ways: DC_{rel} and Φ_{rel} data were simultaneously fit to Eqs. (5) and (7), respectively; AC_{rel} and Φ_{rel} data were simultaneously fit to Eqs. (6) and (7), respectively; and finally Φ_{rel} and M_{rel} data were simultaneously fit to Eqs. (7) and (8), respectively. All the fitting routines we used are part of the commercial

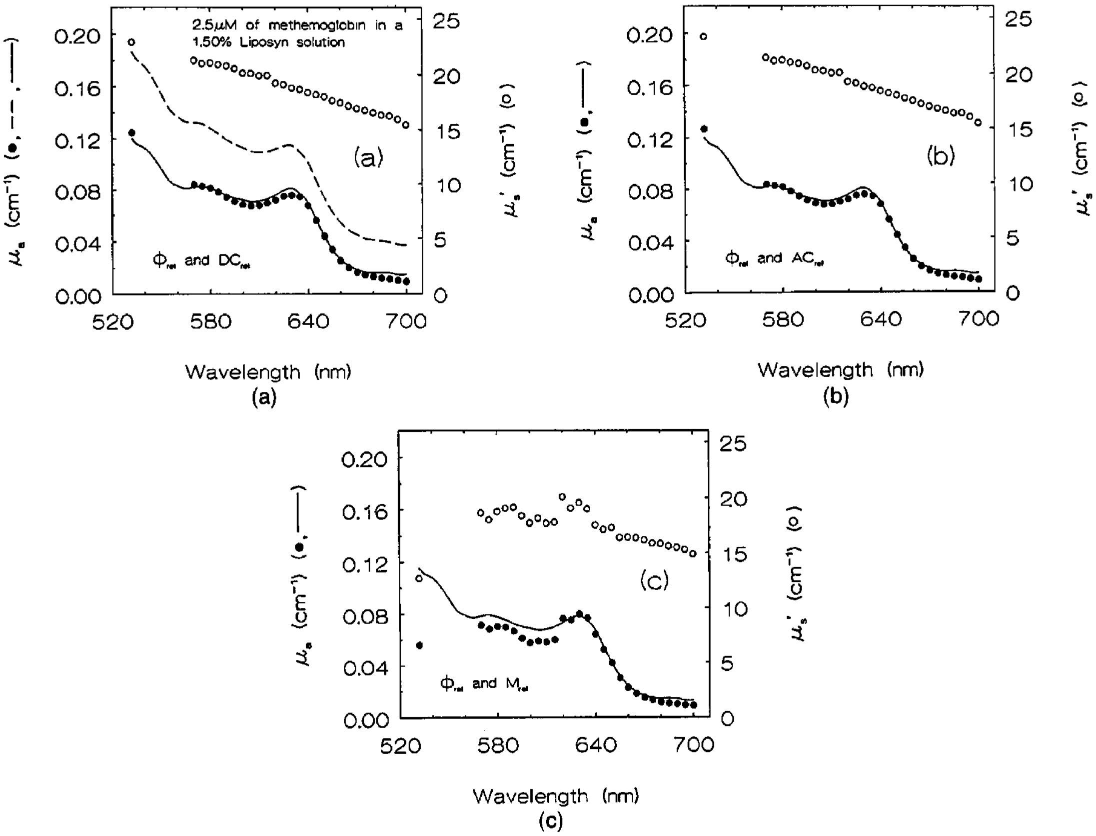

Fig. 6. (a) Frequency-domain-determined scattering and absorption of the 2.5-μM methemoglobin/1.50% Liposyn/7.23 pH aqueous buffer medium. Absolute absorption coefficients μ_a (●) and absolute reduced scattering coefficients μ_s' (○) were determined by simultaneously fitting DC_{rel} and Φ_{rel} data, obtained at two relative distances (i.e., $r = 2.5$ and 3.0 cm relative to $r_0 = 2.0$ cm) at multiple modulation frequencies ranging from 19.05 to 304.80 MHz, to Eqs. (5) and (7), respectively. The uncertainties in the μ_a and μ_s' values recovered from the data analysis are of the order of 5×10^{-4} and 0.1 cm^{-1}, respectively. The dashed curve is the same curve as shown in Fig. 4. The solid curve is the Rayleigh-scattering-corrected methemoglobin absorption spectrum that we obtained by subtracting scattering values determined by Eq. (15) from the dashed curve. (b) Same sample as in (a) except that we determined the medium optical parameters represented by the circles by simultaneously fitting AC_{rel} and Φ_{rel} data to Eqs. (6) and (7), respectively. The uncertainties recovered from the data analysis here are the same as in (a). (c) Same sample as in (a) except that we determined the medium optical parameters represented by the circles by simultaneously fitting Φ_{rel} and M_{rel} data to Eqs. (7) and (8), respectively. The uncertainties in the μ_a and μ_s' values recovered from the data analysis are of the order of 8×10^{-4} and 0.2 cm^{-1}, respectively.

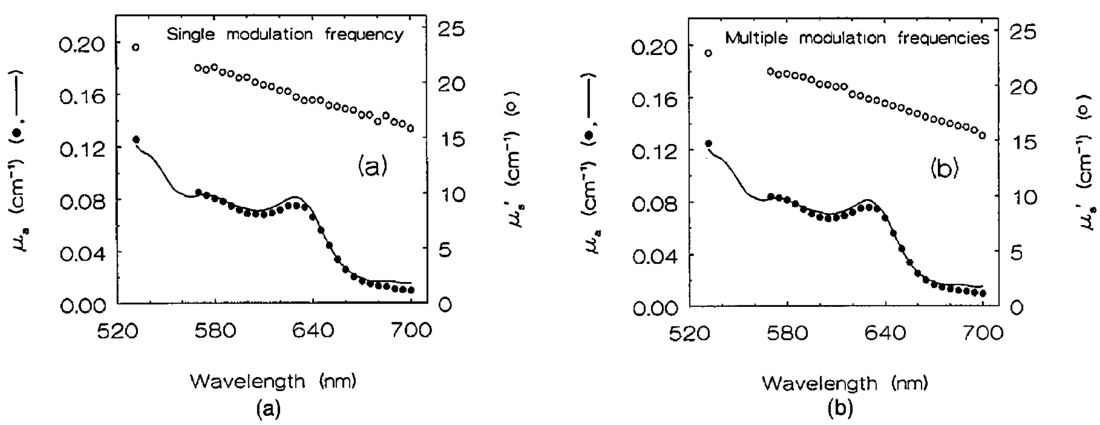

Fig. 7. (a) Same sample as in Fig. 6(a) except that the DC_{rel} and Φ_{rel} data simultaneously fit to Eqs. (5) and (7), respectively, were obtained at a single relative distance (i.e., $r = 2.5$ cm relative to $r_0 = 2.0$ cm) and a single modulation frequency $\omega/2\pi$. At a wavelength of 532 nm, $\omega/2\pi = 228.6$ MHz, and at wavelengths of 570–700 nm, $\omega/2\pi = 114.30$ MHz. The uncertainties in the μ_a and μ_s' values recovered from the data analysis are of the order of 16×10^{-4} and 0.3 cm^{-1}, respectively. (b) Same as Fig. 6(a). Shown for comparison.

package *Globals Unlimited* software (Laboratory for Fluorescence Dynamics, Department of Physics, University of Illinois at Urbana–Champaign).

4.A. Blank Multiple-Scattering Medium

Figure 5 shows spectra of the absolute absorption coefficient and absolute reduced scattering coefficient (i.e., μ_a and μ_s', respectively) obtained for the blank multiple-scattering medium (i.e., no methemoglobin, solids content of 1.54% Liposyn). The μ_a and μ_s' values at a given light-source wavelength λ were extracted from the DC_{rel} and Φ_{rel} data obtained at λ from this blank scattering medium. The uncertainties of the μ_a and μ_s' values are given in the caption of Fig. 5. The μ_a spectrum of the blank multiple-scattering medium (i.e., the solid circles) is compared with values of μ_a for water (i.e., the crosses) given at several wavelengths by Hale and Querry.[29] The order of magnitude of μ_a is the same for both quantities, and their spectral dependence is qualitatively comparable. The measured μ_s' spectrum of Fig. 5 (i.e., open circles) is compared with the solid $\mu_s'(\lambda)$ curve predicted by van Staveren *et al.*[30] for the same amount of solids content on the basis of Mie theory calculations. Although van Staveren *et al.* considered a slightly different scattering medium (i.e., Intralipid 10%, Kabivitrum, Stockholm), it is clear that both the order of magnitude and the spectral dependence of our measured μ_s' values are reproduced by the Mie theory calculations of van Staveren *et al.* Wilson *et al.*[31] obtained results similar to ours when comparing their frequency-domain determined values of μ_s' of a 1% Liposyn solution with the predictions of the Mie theory calculations of van Staveren *et al.*

4.B. Multiple-Scattering Medium Containing 2.5 μM of Methemoglobin

Figures 6 and 7 show spectra of the absolute absorption coefficient μ_a (i.e., the solid circles) resulting from 2.5 μM of methemoglobin uniformly mixed with a 1.50% Liposyn solution and the absolute reduced scattering coefficient μ_s' (i.e., the open circles). The μ_a and μ_s' values shown in Figs. 6(a), 6(b), and 6(c) were obtained, respectively, from Φ_{rel} and DC_{rel}, Φ_{rel} and AC_{rel}, and Φ_{rel} and M_{rel} data. The uncertainties of the μ_a and μ_s' values are given in the captions of Figs. 6 and 7. We obtained the values of μ_a represented by the solid circles by subtracting the values of μ_a measured in the blank medium from the values of μ_a determined for the 2.5-μM methemoglobin/1.50% Liposyn/aqueous buffer solution.

4.B.1. Analysis of Φ_{rel} and DC_{rel} Measurement

We determined the μ_a values shown in Fig. 6(a) at given λ values by extracting the absolute absorption coefficient (and scattering coefficient) of the 2.5-μM methemoglobin/1.50% Liposyn/7.23 pH aqueous buffer solution from the Φ_{rel} and DC_{rel} data acquired from this medium at λ and then subtracting the μ_a value at the same λ in Fig. 5 from this absorption. The values of μ_a represented by the dashed curve in Fig. 6(a) are also given in Fig. 4; i.e., the dashed curve represents the steady-state-determined methemoglobin absorption spectrum $[\mu_a]_{\mathrm{app}}$. Note that the solid circles and the dashed curve follow the same general trend, although a systematic discrepancy between the frequency-domain-determined absorption spectrum and the steady-state-determined absorption spectrum grows larger at lower wavelengths. We believe that this systematic discrepancy is due to Rayleigh scattering. [Note that by employing Eq. (1) to determine the dashed curve from the measured optical density, one determines $[\mu_a]_{\mathrm{app}} \equiv \mu_a + \mu_s$.] Although methemoglobin is an almost spherical molecule of 5.5-nm diameter[32] and scatters light at the wavelengths used, it is likely that the large discrepancy between the steady-state- and frequency-domain-determined absorption spectra is due to scattering from impurities rather than from methemoglobin molecules. Further purification of our methemoglobin samples have provided steady-state-determined spectra that are coincident with the spectra reported in Figs. 6 and 7 that were determined from frequency-domain data. We obtained the solid curve in Fig. 6(a) by subtracting an assumed amount of Rayleigh scattered light from the steady-state-determined spectrum represented by the dashed curve. The amount of Rayleigh scattering subtracted from the dashed curve is given by

$$\mu_s = \frac{\alpha}{\lambda^4}, \tag{15}$$

where α is a constant that is chosen so that the subtraction yields a solid curve, i.e., a Rayleigh-scattering-corrected methemoglobin absorption spectrum, that best fits the solid circles. The solid curves in Figs. 6(b), 6(c), and 7 were determined in an identical fashion, with α chosen to best fit the solid circles in a given figure. The value of α used to obtain the solid curves shown in Figs. 6(a) and 6(b) is 5.3×10^{-19} cm^3, and the value of α used in Fig. 6(c) is 5.7×10^{-19} cm^3. The good agreement between the solid curve (i.e., the Rayleigh-scattering-corrected absorption spectrum) and the solid circles in Fig. 6(a) indicates that the methemoglobin absorption spectrum obtained from the Φ_{rel} and DC_{rel} data is accurately determined. However, unlike for the calculation of the solid curve, we made no assumptions about the type of scattering in calculating the μ_a and μ_s' values from the frequency-domain data, other than that the light transport through the methemoglobin/Liposyn/buffer medium was diffusive and that $\mu_a \ll \mu_s'$ for this medium. The assumption of diffusive light transport allows for the complete separation of all absorption processes (contained in the values of μ_a represented by the solid circles) from all scattering processes (contained in the values of μ_s' represented by the open circles), including Mie scattering from Liposyn particles and Rayleigh scattering from impurities in the methemoglobin sample. The difference between the dashed curve and the solid circles of Fig. 6(a) indicates that in the measurement performed with a steady-state technique and a transmission geometry a significant fraction of the light traversing the 1-cm cuvette fails to reach the detector because of Rayleigh scattering in the 532–700-nm spectral region.

We emphasize that an independent evaluation of the scattering present in the methemoglobin solution (in the absence of Liposyn) was obtained. This scattering was determined from the comparison of the methemoglobin spectrum determined from the frequency-domain method (in the presence of Liposyn) with the methemoglobin spectrum determined from the steady-state method (in the absence of Liposyn). The significant scattering detected in the methemoglobin solution (in the absence of Liposyn) should serve as a caveat to researchers who employ the Beer–Lambert relationship [i.e., Eq. (1)] to determine the absorption spectra of hemoglobin solutions from steady-state measurements of the optical density of these solutions.

4.B.2. *Analysis of the Φ_{rel} and AC_{rel} Measurement*

Figure 6(b) shows the values of μ_a and μ_s' that were extracted from the Φ_{rel} and AC_{rel} data. The μ_a and μ_s' values shown in this figure are almost identical to their respective counterparts in Fig. 6(a), which were calculated from Φ_{rel} and DC_{rel} data. The good agreement between the solid curve (i.e., the Rayleigh-scattering-corrected absorption spectrum) and the solid circles in Fig. 6(b) indicates that the methemoglobin absorption spectrum obtained from the Φ_{rel} and AC_{rel} data is accurately determined.

4.B.3. *Analysis of Φ_{rel} and M_{rel} Measurement*

Figure 6(c) shows the values of μ_a and μ_s' that were extracted from the Φ_{rel} and M_{rel} data. The μ_a values extracted from the Φ_{rel} and M_{rel} data at any given λ (with the exception of the μ_a and μ_s' values obtained at $\lambda = 620$, 625, 630, and 635 nm) are all smaller than their counterparts that were extracted from the Φ_{rel} and DC_{rel} (AC_{rel}) data in Figs. 6(a) and 6(b). At wavelengths between 700 and 640 nm the μ_a and μ_s' values shown in Fig. 6(c) are smaller than the μ_a and μ_s' values shown in Fig. 6(a) [or Fig. 6(b)] by $\sim$5%. At wavelengths between 570 and 615 nm the μ_a and μ_s' values shown in Fig. 6(c) are smaller than the μ_a and μ_s' values shown in Fig. 6(a) [or Fig. 6(b)] by $\sim$15%. This deviation increases to $\sim$50% at 532 nm. This systematic effect cannot be explained by random noise in the frequency-domain measurement. Also, unlike in Figs. 6(a) and 6(b), the μ_a spectrum extracted from the Φ_{rel} and M_{rel} data compares relatively poorly with the Rayleigh-scattering-corrected μ_a spectrum represented by the solid curve. The comparison is particularly poor at wavelengths smaller than 620 nm, with the most dramatic deviation occurring at 532 nm, where the absorption of the methemoglobin determined from the steady-state measurement is largest. In addition, at wavelengths smaller than 660 nm, the fluctuations in the μ_s' spectrum follow the same trend as the fluctuations in the μ_a spectrum.

Clearly the simultaneous nonlinear least-squares fit of the Φ_{rel} and M_{rel} data to Eqs. (7) and (8), respectively, yields a systematically inaccurate description of the scattering and absorption properties of the medium when the absorbing properties of the medium become sufficiently large. This result is surprising because the relative demodulation is given by $M_{\mathrm{rel}} \equiv AC_{\mathrm{rel}}/DC_{\mathrm{rel}}$, and the AC_{rel} and DC_{rel} data yield reasonable results when used separately in conjunction with the Φ_{rel} data for the calculation of μ_a and μ_s' [see Figs. 6(a) and 6(b)]. The greater contribution to the uncertainty in μ_a and μ_s' from the M_{rel} data (used with the Φ_{rel} data) compared with the contribution to the uncertainty in these quantities from the AC_{rel} or DC_{rel} data (used with the Φ_{rel} data) does not explain the phenomena shown in Fig. 6(c), namely, why the values of μ_a represented by the solid circles show a significant systematic deviation from the solid curve at larger absorption values or why the fluctuations in the μ_s' spectrum correlate with the fluctuations in the μ_a spectrum at larger absorption values. We mention here that the values of μ_a and μ_s' that were extracted from the DC_{rel} and AC_{rel} data by simultaneously fitting these quantities to Eqs. (5) and (6), respectively, also show systematically inaccurate behavior when compared with any Rayleigh-scattering-corrected, steady-state-determined absorption spectrum.

4.C. Single-Modulation-Frequency Measurement Versus Multiple-Modulation-Frequency Measurement

Figure 7(a) shows values of μ_a and μ_s' extracted from DC_{rel} and Φ_{rel} data acquired at a single intensity-modulation frequency in the 2.5-μM methemoglobin/1.50% Liposyn/7.23 pH aqueous buffer solution. Equations (5) and (7) were used for this calculation with $r = 2.5$ cm, $r_0 = 2.0$ cm and with $\omega/2\pi = 228.6$ MHz at $\lambda = 532$ nm and 114.3 MHz at $\lambda = 570$–700 nm. Figure 7(b) shows μ_a and μ_s' values that were determined by simultaneously fitting from DC_{rel} and Φ_{rel} data obtained at multiple modulation frequencies to Eqs. (5) and (7), respectively. [The μ_a and μ_s' values obtained in this manner as well as the solid curve are also shown in Fig. 6(a).] The results in Fig. 7(a) are almost identical to the results in Fig. 7(b), albeit the μ_a and μ_s' values (particularly the μ_s' values) in Fig. 7(a) are slightly noisier and their uncertainties are approximately three times larger than the uncertainties in the points in Fig. 7(b) [see the Fig. 6(a) caption for the errors in the Fig. 7(b) parameters]. The greater noise and larger uncertainties are not surprising, given that only one-tenth of the data set that was used in calculating the μ_a and μ_s' values in Fig. 7(b) was used to calculate the μ_a and μ_s' values in Fig. 7(a). The greater noise notwithstanding, a comparison of the spectra in Fig. 7(a) with the spectra in Fig. 7(b) indicates that a single, properly chosen light-intensity-modulation frequency $\omega/2\pi$ will suffice to determine accurately the absorp tion spectrum of a tissuelike phantom from the Φ_{rel} and DC_{rel} (AC_{rel}) data. [A properly chosen modulation frequency is such that for a given value of $(r - r_0)$ the signal-to-noise ratio is maximized for the particular pair of variables used.] Comparatively rapid acquisition of the absorption and scattering spectra of tissuelike phantoms is thereby possible, because measurement at a single modulation frequency is sufficient.

5. Discussion

To obtain some feeling for how different values of μ_a and μ_s' are extracted from different combinations of DC_{rel}, AC_{rel}, and Φ_{rel} data, contours of constant DC_{rel}, AC_{rel}, Φ_{rel}, and M_{rel} are plotted in Fig. 8 from Eqs. (11)–(14). Frequency-domain data acquired from the 2.5-μM methemoglobin/1.50% Liposyn/7.23 pH aqueous buffer medium with a light-source wavelength of 605 nm at light-intensity modulation frequencies of 92.25 and 190.50 MHz were used in these calculations. These 605-nm data exhibit behavior that is the same as the behavior of the data at most other wavelengths and modulation frequencies. The values of the data (i.e., DC_{rel}, AC_{rel}, Φ_{rel}, and M_{rel}) and the source/detector separations (i.e., r and r_0) used in these calculations are given in the caption of Fig. 8. The intersection of a pair of curves in Fig. 8 yields a value of μ_a and a value of μ_s' that together satisfy the two equations used to calculate those curves. Ideally in a noiseless system a diffusive medium with specific values of μ_a and μ_s' at a given λ would yield specific frequency-domain data (i.e., specific values for DC_{rel}, AC_{rel}, Φ_{rel}, and M_{rel} at given values of r, r_0, and $\omega/2\pi$) that would in turn yield four curves generated from Eqs. (11)–(14), all intersecting at the same point. Our frequency-domain data do not yield this result, as can be seen in Fig. 8. Regardless of the modulation frequency, our data yield intersection points of the contours of constant DC_{rel}, AC_{rel}, Φ_{rel}, and M_{rel}, which always have the same relative orientation on the μ_a–μ_s' plane. For example, in Fig. 8(a), the intersection of the Φ_{rel} and M_{rel} curves yields μ_a and μ_s' values that are 0.051 and 14.4 cm^{-1}, respectively, whereas the intersection of the Φ_{rel} curve with the AC_{rel} or DC_{rel} curve yields μ_a and μ_s' values that are 0.075 and 20.5 cm^{-1}, respectively. The intersection of the AC_{rel} curve with the DC_{rel} curve in Fig. 8(a) yields μ_a and μ_s' values that are 0.062 and 24.0 cm^{-1}, respectively. However by comparing Fig. 8(a) with Fig. 8(b), we see that the ideal case of a common intersection point for all the contours is more closely approximated at the higher light-intensity-modulation frequency.

The systematic behavior of the intersection points in Fig. 8 illustrates the consistently low (and inaccurate) values obtained for μ_a and μ_s' in Fig. 6(c) compared, respectively, with the μ_a and μ_s' values shown in Figs. 6(a) and 6(b). The systematic deviation between the intersection point of the Φ_{rel} and DC_{rel} curves and the intersection point of the Φ_{rel} and AC_{rel} curves is relatively small, and in any case both of these data sets yield reasonably accurate absorption spectra, as can be seen in Figs. 6(a), 6(b), and 7. The relatively gross systematic inaccuracy of the spectra in Fig. 6(c) [compared with the spectra in Figs. 6(a) and 6(b)], which increases with increasing absorption, appears to arise from the relative behavior of the DC_{rel} and AC_{rel} data, with the size of this effect being magnified at lower modulation frequencies, where the DC_{rel} and AC_{rel} data are correspondingly closer in value. The intersection point of the Φ_{rel} and M_{rel} contours is affected by the relative behavior of the DC_{rel} and AC_{rel} data because $M_{\mathrm{rel}} \equiv AC_{\mathrm{rel}}/DC_{\mathrm{rel}}$. Because $M_{\mathrm{rel}} \equiv AC_{\mathrm{rel}}/DC_{\mathrm{rel}}$, the contours of constant AC_{rel}, DC_{rel}, and M_{rel} intersect at the same point. A small systematic shift in the orientation of the AC_{rel} contour relative to the DC_{rel} contour in the μ_a–μ_s' plane leads to a relatively large shift of the intersection point of the contours of constant AC_{rel}, DC_{rel}, and M_{rel}, which in turn leads to a large systematic shift in the location of the intersection point between the contours of constant Φ_{rel} and M_{rel}.

The systematic inaccuracy of the spectra extracted from the Φ_{rel} and M_{rel} data or from the DC_{rel} and AC_{rel} data has several possible origins:

(a) An unaccounted for instrumental artifact in our frequency-domain spectrophotometer introduces a slight systematic deviation in the DC_{rel} data relative to the AC_{rel} data, which becomes less evident in our frequency-domain diffusion model at higher modulation frequencies, as shown in Fig. 8. One possible effect that we considered was connected to the 0.3-cm

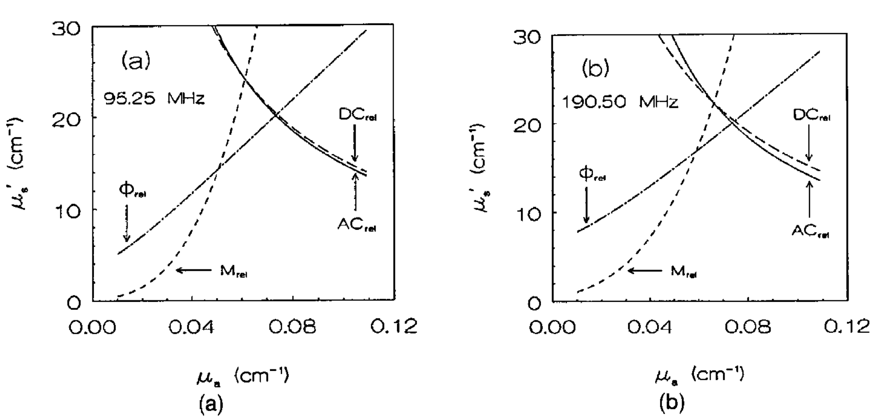

Fig. 8. (a) Plots of Eqs. (11)–(14) with frequency-domain data: $DC_{\mathrm{rel}} = 0.278$, $AC_{\mathrm{rel}} = 0.271$, $\Phi_{\mathrm{rel}} = 10.74°$, and $M_{\mathrm{rel}} = 0.975$. The data were obtained from the 2.5-μM methemoglobin/1.50% Liposyn/7.23 pH aqueous buffer medium at $\lambda = 605$ nm, $\omega/2\pi = 95.25$ MHz and at $r = 2.5$ cm relative to $r_0 = 2.0$ cm. (b) Same as (a) except that $\omega/2\pi = 190.50$ MHz and $DC_{\mathrm{rel}} = 0.279$, $AC_{\mathrm{rel}} = 0.260$, $\Phi_{\mathrm{rel}} = 20.56°$, and $M_{\mathrm{rel}} = 0.932$.

diameter of the detector optical fiber (i.e., optical fiber Fd in Fig. 3). We have assumed in our measurements that the detector optical fiber with the 0.3-cm-diameter aperture measures the properties of a photon-density wave [i.e., $DC(r)$, $AC(r)$, $\Phi(r)$, and $M(r)$] at a precise distance r from an isotropically emitting point source in an infinite medium. Assuming for the moment that our model of the light source and medium boundaries is completely accurate, the measurement geometry that we employ (see Fig. 2) actually permits the detector optical fiber to sample a continuously distributed light intensity that decays exponentially with r, divided by r, across the 0.3-cm-diameter fiber aperture and is continuously shifted in phase across this aperture according to Eq. (2). With this premise in mind, we considered the possibility that our assumption of a single r value for a given set of frequency-domain data in these circumstances could cause the results from our diffusion model to be skewed in one particular direction and skewed slightly differently for the AC data compared with the DC data. We disregarded this possibility after we reduced the diameter of our collection optics to 0.1 cm and observed that no significant change occurred in the above-mentioned systematic behavior.

(b) The analytical model we employ fails to describe our system with complete accuracy. Specific inaccuracies within the analytical model may be the following: (1) With the model that we use we assume that we have an isotropically emitting point source of light, with this light source located approximately one mean free path from the end of the source optical fiber (i.e., optical fiber Fs in Fig. 3). This may not be a completely accurate assumption, given that the distance of the end of the detector optical fiber ranges from 2.0 to 3.0 cm from the end of the source optical fiber. In this region the source may be more accurately modeled as a distributed entity that injects light in one direction into the scattering medium. (2) The scattering medium in which we perform our measurements is not infinite, but with our model we assume an infinite medium. Escaping light from the scattering medium is visible by eye, and the application of the infinite geometry diffusion model to this medium is thereby not completely accurate. We disregard this as a possible source of inaccuracy of our spectra when we note that the largest systematic error is observed at a wavelength where the mean free path of a photon in the medium is smallest.

(c) The diffusion approximation that is represented by Eq. (2) has some limits.[19] In Eq. (2) we give a most accurate description of the light transport when the albedo of the medium [i.e., $\mu_s/(\mu_a + \mu_s)$] is close to unity, i.e., $\mu_s \gg \mu_a$. In Fig. 6 the ratio μ_s'/μ_a decreases from $\mu_s'/\mu_a \approx 900$ at 700 nm to $\mu_s'/\mu_a \approx 200$ at 532 nm. This result indicates that it may not be coincidental that the magnitude of the systematic behavior observed in the μ_s' and μ_a spectra obtained from the demodulation data increases with increasing absorption.

Figure 9 demonstrates how a frequency-domain measurement at a single properly chosen modulation frequency suffices to extract accurately the optical properties of a tissuelike phantom by simultaneously fitting the DC_{rel} and Φ_{rel} data to Eqs. (5) and (7), respectively. The five contours of constant Φ_{rel} and the one contour of constant DC_{rel} in this figure are calculated from the data acquired from the 2.5-μM methemoglobin/1.50% Liposyn/7.23 pH aqueous buffer medium at a 605-nm wavelength, with $r = 2.5$ cm, $r_0 = 2.0$ cm and with $\omega/2\pi = 95.25$, 114.30, 152.40, 190.50, and 247.65 MHz. The Φ_{rel} value associated with each $\omega/2\pi$ value, as well as the DC_{rel} value, is given in the caption of Fig. 9. We performed the calculations for this figure using Eqs. (11) and (13). A simultaneous fit of all the multifrequency Φ_{rel} data to Eq. (7) yields optical parameters from our data set (obtained in the modulation-frequency range of 19.05–304.80 MHz), which are less well determined than those extracted from a simultaneous fit of the DC_{rel} and Φ_{rel} data acquired at a single modulation frequency to Eqs. (5) and (7), respectively. A simultaneous fit of the DC_{rel} and multifrequency Φ_{rel} data to Eqs. (5) and (7), respectively, yields smaller confidence limits than those that we obtained by fitting the DC_{rel} and Φ_{rel} data acquired at a single modulation frequency to Eqs. (5) and (7), respectively [see Figs. 6(a) and 7(a)]. If a sufficiently large modulation-frequency range is used (for example, ~100 MHz to 1 GHz), a simultaneous fit of multifrequency Φ_{rel} data to Eq. (7) might yield optical parameters that are as well determined as those determined by a simultaneous fit of our DC_{rel} and Φ_{rel} data acquired at a single modulation frequency to Eqs. (5) and (7), respectively. However, note that at modulation frequencies of the order of or greater than 1 GHz, Eq. (2) no longer provides an accurate description of photon-density waves in a tissuelike phantom, and a higher-order diffusion approximation is needed to describe more accurately the propagation of photon-density waves in tissuelike media.[19,33]

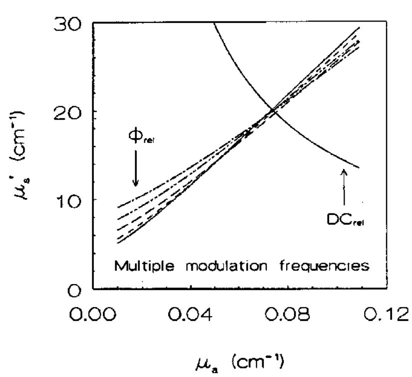

Fig. 9. Plots of Eqs. (11) and (13) with frequency-domain data obtained from the 2.5-μM methemoglobin/1.50% Liposyn/7.23 pH aqueous buffer medium at $\lambda = 605$ nm and at $r = 2.5$ cm relative to $r_0 = 2.0$ cm. These data are as follows: $DC_{\mathrm{rel}} = 0.278$; at $\omega/2\pi = 95.25$ MHz, $\Phi_{\mathrm{rel}} = 10.74°$; at $\omega/2\pi = 114.30$ MHz, $\Phi_{\mathrm{rel}} = 12.71°$; at $\omega/2\pi = 152.40$ MHz, $\Phi_{\mathrm{rel}} = 16.53°$; at $\omega/2\pi = 190.50$ MHz, $\Phi_{\mathrm{rel}} = 20.56°$; at $\omega/2\pi = 247.65$ MHz, $\Phi_{\mathrm{rel}} = 25.89°$. The Φ_{rel} curves [i.e., the curves generated by Eq. (13)] become more horizontal with increasing modulation frequency.

6. Conclusion

In this frequency-domain study we have presented evidence that the relative phase shift (i.e., Φ_{rel}) data used in conjunction with the DC_{rel} data or alternatively the Φ_{rel} data used in conjunction with the AC_{rel} data yield accurate absolute absorption coefficient spectra of turbid media. The Φ_{rel} data used in conjunction with the relative demodulation (i.e., $M_{rel} \equiv AC_{rel}/DC_{rel}$) data yield relatively less accurate absolute absorption coefficient spectra of turbid media. An infinite medium, frequency-domain diffusion model with an isotropically emitting point source of light was employed to extract the absolute optical properties of the turbid medium from our frequency-domain data. We confirmed the accuracy of the model by comparing the frequency-domain-determined methemoglobin absorption spectrum in a tissuelike phantom to a steady-state-determined methemoglobin absorption spectrum in a minimally scattering medium, which is corrected for Rayleigh scattering. We have demonstrated that simultaneously fitting data acquired at multiple modulation frequencies ranging from 19.05 to 304.80 MHz offers no significant improvement in the noise or accuracy of the measured absorption spectra.

Figures 6(a) and 6(b) show that we can separate Rayleigh scattering that contributes to the apparent absorption spectrum from a steady-state measurement in the visible spectral region from the absorption of the methemoglobin molecules by using frequency-domain techniques, provided that the methemoglobin is uniformly distributed in a multiple-scattering medium. Paradoxically, we have corrected the steady-state-determined methemoglobin absorption spectrum for scattering by impurities in the methemoglobin by adding more scattering.

These experiments and analyses of the data produced were performed at the Laboratory for Fluorescence Dynamics (LFD) in the Department of Physics at the University of Illinois at Urbana–Champaign (UIUC). The LFD and this research are supported by the National Institutes of Health (RR03155 and CA57032) and by UIUC. The authors thank Julia K. Butzow for help in preparing this manuscript, John Maier for creating Fig. 2, and Gerd U. Nienhaus and Theodore L. Hazlett for advice about the preparation of the methemoglobin solutions.

References

1. Three special journal issues on biomedical optics: Appl. Opt. **28,** 2207–2357 (1989); Appl. Opt. **32,** 367–627 (1993); Opt. Eng. **32,** 244–266 (1993).
2. G. Müller, B. Chance, R. Alfano, S. Arridge, J. Beuthan, E. Gratton, M. Kaschke, B. Masters, S. Svanberg, P. van der Zee, and R. F. Potter, eds., *Medical Optical Tomography: Functional Imaging and Monitoring,* Proc. Soc. Photo-Opt. Instrum. Eng. **IS11,** 3–642 (1993).
3. B. Chance, ed., *Photon Migration in Tissue* (Plenum, New York, 1989), pp. 1–195.
4. K. M. Yoo, F. Liu, and R. R. Alfano, "Biological materials probed by the temporal and angular profiles of the backscattered ultrafast laser pulses," J. Opt. Soc. Am. B **7,** 1685–1693 (1990).
5. B. Chance, S. Nioka, J. Kent, K. McCully, M. Fountain, R. Greenfeld, and G. Holtom, "Time-resolved spectroscopy of hemoglobin and myoglobin in resting and ischemic muscle," Anal. Biochem. **174,** 698–707 (1988).
6. M. Cope and D. T. Delpy, "System for long-term measurement of cerebral blood and tissue oxygenation on newborn infants by near infrared transillumination," Med. Biol. Eng. Comput. **26,** 289–294 (1988).
7. M. S. Patterson, B. C. Wilson, J. W. Feather, D. M. Burns, and W. Pushka, "The measurement of dihematopotphyrin ether concentration in tissue by reflectance spectrophotometry," Photochem. Photobiol. **46,** 337–343 (1987).
8. S. L. Jacques and S. A. Prahl, "Modeling optical and thermal distribution in tissue during laser irradiation," Laser Surg. Med. **6,** 494–503 (1987).
9. E. Gratton, W. W. Mantulin, M. J. vandeVen, J. B. Fishkin, M. B. Maris, and B. Chance, "The possibility of a near-infrared optical imaging system using frequency-domain methods," in *Proceedings of the Third International Conference on Peace through Mind/Brain Science* (Hamamatsu, Hamamatsu City, Japan, 1990), pp. 183–189.
10. J. B. Fishkin, E. Gratton, M. J. vandeVen, and W. W. Mantulin, "Diffusion of intensity-modulated near-infrared light in turbid media," in *Time-Resolved Spectroscopy and Imaging of Tissues,* B. Chance and A. Katzir, eds., Proc. Soc. Photo-Opt. Instrum. Eng. **1431,** 122–135 (1991).
11. B. J. Tromberg, L. O. Svaasand, T. Tsay, and R. C. Haskell, "Properties of photon density waves in multiple-scattering media," Appl. Opt. **32,** 607–616 (1993).
12. L. O. Svaasand, B. J. Tromberg, R. C. Haskell, T. Tsay, and M. W. Berns, "Tissue characterization and imaging using photon density waves," Opt. Eng. **32,** 258–266 (1993).
13. A. Duncan, T. L. Whitlock, M. Cope, and D. T. Delpy, "A multiwavelength, wideband, intensity modulated optical spectrometer for near-infrared spectroscopy and imaging," in *Photon Migration and Imaging in Random Media and Tissues,* B. Chance and R. R. Alfano, eds., Proc. Soc. Photo-Opt. Instrum. Eng. **1888,** 248–257 (1993).
14. A. H. Hielscher, F. K. Tittel, and S. L. Jacques, "Noninvasive monitoring of blood oxygenation by phase resolved transmission spectroscopy," in *Photon Migration and Imaging in Random Media and Tissues,* B. Chance and R. R. Alfano, eds., Proc. Soc. Photo-Opt. Instrum. Eng. **1888,** 275–288 (1993).
15. W. Cui and L. E. Ostrander, "Effect of local changes on phase shift measurement using phase modulation spectroscopy," in *Photon Migration and Imaging in Random Media and Tissues,* B. Chance and R. R. Alfano, eds., Proc. Soc. Photo-Opt. Instrum. Eng. **1888,** 289–296 (1993).
16. E. M. Sevick, B. Chance, J. Leigh, S. Nioka, and M. Maris, "Quantitation of time- and frequency-resolved optical spectra for the determination of tissue oxygenation," Anal. Biochem. **195,** 330–351 (1991).
17. M. S. Patterson, J. D. Moulton, B. C. Wilson, K. W. Berndt, and J. R. Lakowicz, "Frequency-domain reflectance for the determination of the scattering and absorption properties of tissues," Appl. Opt. **30,** 4474–4476 (1991).
18. S. Fantini, M. A. Franceschini, J. B. Fishkin, B. Barbieri, and E. Gratton, "Quantitative determination of the absorption spectra of chromophores in strongly scattering media: light-emitting-diode-based technique," Appl. Opt. **33,** 5204–5213 (1994).
19. J. B. Fishkin and E. Gratton, "Propagation of photon-density waves in strongly scattering media containing an absorbing semi-infinite plane bounded by a straight edge," J. Opt. Soc. Am. A **10,** 127–140 (1993).

20. K. M. Case and P. F. Zweifel, *Linear Transport Theory* (Addison-Wesley, Reading, Mass., 1967), Chap. 2, p. 17.
21. J. J. Duderstadt and W. R. Martin, *Transport Theory* (Wiley, New York, 1979), Chap. 2, p. 66.
22. M. S. Patterson, B. Chance, and B. C. Wilson, "Time resolved reflectance and transmittance for the noninvasive measurement of tissue optical properties," Appl. Opt. **28,** 2331–2336 (1989).
23. J. R. Alcala, E. Gratton, and D. M. Jameson, "A multifrequency phase fluorometer using the harmonic content of a mode-locked laser," Anal. Instrum. **14,** 225–250 (1985).
24. B. A. Feddersen, D. W. Piston, and E. Gratton, "Digital parallel acquisition in frequency domain fluorometry," Rev. Sci. Instrum. **60,** 2929–2936 (1989).
25. B. Barbieri, F. De Piccoli, M. vandeVen, and E. Gratton, "What determines the uncertainty of phase and modulation measurements in frequency domain fluorometry," in *Time Resolved Laser Spectroscopy in Biochemistry II,* J. R. Lakowicz, ed., Proc. Soc. Photo-Opt. Instrum. Eng. **1204,** 158–170 (1990).
26. R. Lemberg and J. W. Legge, *Hematin Compounds and Bile Pigments* (Interscience, New York, 1949), Chap. 6, p. 218.
27. W. F. Cheong, S. A. Prahl, and A. J. Welch, "A review of the optical properties of biological tissues," IEEE J. Quantum Electron. **26,** 2166–2185 (1990).
28. J. M. Beechem and E. Gratton, "Fluorescence spectroscopy data analysis environment: a second generation global analysis program," in *Time-Resolved Laser Spectroscopy in Biochemistry,* J. R. Lakowicz, ed., Proc. Soc. Photo-Opt. Instrum. Eng. **909,** 70–82 (1989).
29. G. M. Hale and M. R. Querry, "Optical constants of water in the 200-nm to 200-μm wavelength region," Appl. Opt. **12,** 555–563 (1973).
30. H. J. van Staveren, C. J. M. Moes, J. van Marle, S. A. Prahl, and M. J. C. van Gemert, "Light scattering in Intralipid-10% in the wavelength range of 400–1100 nm," Appl. Opt. **30,** 4507–4514 (1991).
31. B. C. Wilson, M. S. Patterson, and B. W. Pogue, "Instrumentation for *in vivo* tissue spectroscopy and imaging," in *Medical Lasers and Systems II,* D. M. Harris and C. M. Penney, eds., Proc. Soc. Photo-Opt. Instrum. Eng. **1892,** 132–147 (1993).
32. L. Stryer, *Biochemistry* (Freeman, New York, 1975), Chap. 7, p. 151.
33. J. B. Fishkin, "Imaging and spectroscopy of tissuelike phantoms using photon density waves: theory and experiments," Ph.D. dissertation (University of Illinois at Urbana–Champaign, Urbana, Ill., 1994), Chap. 5, pp. 107–115.